Experimental Evaluation of a Pilot-Scale Thermocline Thermal Energy Storage Combining Latent and Sensible Materials

Muhammad Asaad Keilany[1,2][https://orcid.org/0000-0003-0046-4393], Gilles Flamant[2][https://orcid.org/0000-0003-4562-8515], Mathieu Milhé[1][https://orcid.org/0000-0001-6947-0623], Quentin Falcoz[2], and Jean-Jacques Bézian[1][https://orcid.org/0000-0001-5667-2488]

[1] Centre RAPSODEE, Université de Toulouse ; Ecole des Mines d'Albi, CNRS, Albi F-81013, France.

[2] CNRS-PROMES, 7 Rue du Four Solaire, 66120 Font Romeu-Odeillo, France.

Abstract. This work presents the experimental evaluation of pilot-scale thermocline that integrates a layer of phase change material (PCM) at the top of a sensible heat storage material in a thermocline thermal energy storage (TES) tank. The TES is integrated to the MicroSol-R parabolic trough pilot plant at the PROMES research facility in Odeillo, France. The tank is filled with alumina spheres as sensible heat storage. The PCM is $NaNO_3$ encapsulated in stainless steel horizontal tubes that fill about 5.5% of the tank volume. The charge is evaluated at three mass flow rates 2600, 3000, and 3900 kg/h at two different operating temperature ranges 285-315 ºC and 295-330 ºC. The discharge is studied at three mass flow rates 1600, 2000, and 3000 kg/h from 315 to 220 ºC and 330 to 225 ºC. The performance of the TES is analyzed with two main indicators: the thermocline thickness and the efficiency during the charge and discharge. The results indicate that lower mass flow rates during the charging process result in smaller thermocline thickness. Similarly, during discharge, the thermocline thickness reduces with lower discharge rates. Efficiency evaluation during discharge suggests that an optimal flow rate could be achieved.

Keywords: Thermocline Combined Thermal Energy Storage, Latent-Sensible, Concentrated Solar Power

1. Introduction

Thermocline thermal energy storage (TES) is an economically viable solution for concentrated solar power plants (CSP), Desai et al. [1]. When solid filler is introduced within the tank to increase its thermal capacity, a layer of thermal gradient appears at the frontier between hot and cold heat transfer fluid (HTF). This layer is known as thermocline thickness and it is attributed to additional thermal diffusion within the tank due to the heat exchange between the HTF and the solid filler, Keilany et al. [2]. The stored energy in this layer is a low grade energy, thus thermocline thickness negatively influences the overall performance of the TES. One of the solutions to reduce the thermocline thickness is to combine latent and sensible materials in the same tank, which allows extending the thermal capacity as well as discharge duration, while keeping a relatively constant outlet temperature during the discharge process. The advantage of such combination is using the constant temperature heat release of the PCM during the melting/solidification phase due to its latent heat of fusion.

Ahmed et al. [3] used one-dimensional Schumann model to compare three configurations of thermocline TES. Namely, (1) a reference tank filled only with solid rod as sensible heat storage, (2) a thermocline that is filled only with PCM spheres, and (3) a combination between the two. The thermocline operates between 135 – 195 ºC, while the fusion temperature of the PCM is 165 ºC. They suggested that a combined solution provides a competitive cost reduction of the fully-filled PCM thermocline while it perform better that the sensible heat TES.

A numerical model was developed by Hernández et al. [4] of a combined PCM layer of AlSi at the top of steel slag (sensible heat storage) in a thermocline TES. The operating conditions of the HTF are 27-597 ºC while the fusion temperature is 576 ºC. They studied various combinations of PCM ratio of the TES 0%, 1%, 2.5%, 5%, 10%, and 20%, and concluded that 5% is the recommended ratio.

Zanganeh et al. [5] simulated three ratio of 0.67%, 1.33%, and 2.67% PCM with three different PCMs in the same thermocline TES for HTF running between 590 and 650 ºC. They indicated that 1.33% PCM ratio has the best discharge efficiency at all three tested PCMs. Then Zanganeh et al. [6] developed an experimental setup of 1.33% $AlSi_{12}$ (PCM) with rocks. The PCM is encapsulated within a bundle of stainless-steel tubes placed in staggered positions. They found that the discharge lasted for about 28.5% longer with this combination compared to the sensible heat TES only, with a stabilized outlet temperature at about the PCM melting point.

While there are only few studies that only numerically evaluated such solution, experimental data are scarce. This work presents the experimental evaluation of pilot-scale thermocline that integrates a layer of phase change material (PCM) at the top of sensible heat storage material in the thermocline.

2. Experiment

The thermocline storage for applied research (TSAR) is integrated to the MicroSol-R facility at the PROMES-CNRS research center in Odeillo (France), **Figure 1**.
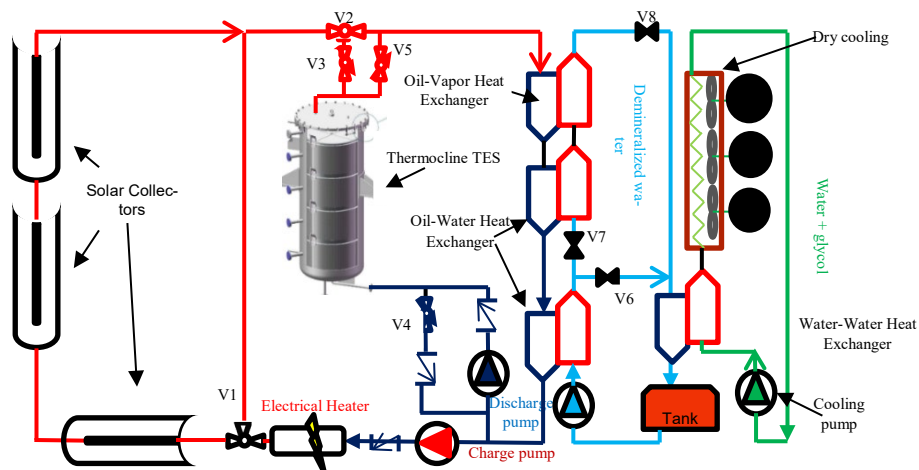

Figure 1. Schematic of MicroSol-R pilot plant.

The thermocline is a 3.3 m^3 tank filled with 4.66 tons of alumina spheres as sensible heat storage, and 337 kg of $NaNO_3$ as PCM. The PCM is encapsulated in a stainless steel horizontal tube that fills about 5.5% of the thermocline volume, Keilany et al. [7].

The sodium nitrate $NaNO_3$ melts at 306 ºC [8], [9] and latent heat of fusion is about 169 kJ/kg. It is commonly used in agriculture application with purity >99% and it has a relatively low cost [10]. This PCM was found compatible to be used with stainless steel 304L encapsulation [11]. Furthermore, this stainless steel has an acceptable decay rate of 6-15 µm/ year at 570ºC when experimented with $NaNO_3$ [12], which is higher than the operating condition of this work.

Materials thermo-physical properties variation with temperature are given Table 1.

Table 1. Temperature dependence thermos-physical properties of storage materials

Property	Jarytherm® oil	Alumina Spheres [13][14]	NaNO$_3$ [15]	SS304
Density ρ [kg/m³]	1261.569 - 0.7419173T	$1000 (3.9853 - (7.158^{-5}(T-273.15))- (3.035^{-8}(T-273.15)^2) + (7.232^{-12}(T-273.15)^3))$	Solid phase: 2160 Liquid phase: 1908	8030
Heat Capacity Cp [J/kg.K]	649.84+ 3.1872180451T	$1117+0.14T – 411exp(-0.006T)$	444.53 + 2.18T	502.48
Thermal conductivity k [W/m.K]	0.1521663 - 8.2406015038^{-5} T	$(-2.469^{-8} T^3) + (9.509^{-5} T^2) - (0.124T) +61.76$	0.3057 + 4.47^{-4} T	16
Dynamic viscosity µ [kg/m.sec]	$exp(19.75102[ln(T)]^4- 492.2114[ln(T)]^3 + 4602.039[ln(T)]^2- 19136.34[ln(T)] +29858.54)$	-	-	-
Latent heat of fusion [kJ/kg]	-	-	169	-

The charge is evaluated at three mass flow rates 2700, 3100, and 3900 kg/h at two different operating temperatures 285-315 ºC and 295-330 ºC. The discharge is studied at three mass flow rates 1600, 2000, and 3000 kg/h from 315 to 220 ºC and from 330 to 225 ºC, respectively.

3. Performance parameters

This work evaluates the performance of a TES based on two criteria: thermocline thickness and charge and discharge efficiency. To define these parameters, the charge and discharge threshold values must be explained as follow.

During the operation of the TES, T$_{high}$ indicates the highest temperature of the HTF and T$_{low}$ the lowest one. The charge threshold T_{thr,c,k_c} represents the maximum HTF temperature at the TES outlet that could be flowed back to the solar filed loop (charging loop). Above this temperature, the charge should be stopped to avoid damaging the solar receiver [2]. It is by equation (1), where the charge factor k_c is usually chosen based on the specifications of the solar field, for benchmarking it is selected at 20% according to Fasquelle et al. [16]

$$T_{thr,c,k_c} = T_{low} + k_c(T_{high} - T_{low}) \tag{1}$$

During discharge, the lowest HTF temperature at the TES outlet that the downstream thermal process can use is identified by equation (2) as T_{thr,d,k_d}. The discharge factor k_d is related to the operation of the downstream process, such as the steam generator temperature, and could be also considered for evaluation purposes at 20% Fasquelle et al. [16].

$$T_{thr,d,k_d} = T_{high} - k_d(T_{high} - T_{low}) \tag{2}$$

1.1 Thermocline thickness

The thermocline thickness size is the height of the zone inside the tank that is bounded by the two threshold temperatures during charge and discharge, equation (3).

$$Th = H(T_{thr,d,20\%}) - H(T_{thr,c,20\%}) \tag{3}$$

The relative thermocline thickness is the ratio between the thermocline thickness-size to the total tank height, equation (4).

$$\delta = \frac{Th}{H_{Tank}} \tag{4}$$

The thermocline thickness is required to be as small as possible because large thermocline thicknesses characterize low TES efficiency as suggested by Bonanos et al. [17].

1.2 Charge efficiency

The charge efficiency is the ratio between the accumulated energy and the maximum potential stored energy in the tank, equations (5)

$$\eta_{charge}(t) = \frac{E_{acc}(t)}{E_{max}} = \frac{E_{acc}(t)_f + E_{acc}(t)_p + E_{acc}(t)_{PCM}}{E_{max_f} + E_{max_p} + E_{max_{PCM}}} \tag{5}$$

The accumulated energy is calculated for each filler material in accordance with its related thermo-physical properties porosity and volume, equation (6)

$$E_{acc}(t) = \int_0^H (A_{int}\varepsilon(\rho.Cp)).(T_{(z,t)} - T_{low}).dz \tag{6}$$

The maximum potential energy is calculated by equation (7).

$$E_{max} = V(1-\varepsilon)(\rho.Cp)(T_{high} - T_{low}) \tag{7}$$

The accumulated energy and the maximum potential energy of PCM are calculated from equations (8) and (9), respectively.

$$E_{acc}(t)_{PCM} = \int_0^{H_{PCM}} A_{int}(1-\varepsilon_{PCM})\rho_{PCM}.L_{fus}dz \tag{8}$$

$$E_{max\,PCM} = V_{tank,PCM}(1-\varepsilon_{PCM})\rho_{PCM}L_{fus} \tag{9}$$

1.3 Discharge efficiency

The discharge efficiency is the ratio of discharged energy to the maximum energy stored in the system at the initial stage, equation (10).

$$\eta_{discharge}(t) = \frac{E_{discharge}(t)}{E_{max}} \tag{10}$$

Where

$$E_{discharge}(t) = \int_0^t m_f.Cp_f.\left(T_{(outlet,t)}-T_{low}\right).dt \tag{11}$$

4. Results and Discussion

4.1 Thermocline thickness

Figure 2 plots the thermocline thickness evolution in time during charges (a) from 285 – 315 °C and (b) from 295 -330°C at the three tested HTF mass flow rates. The results indicate that lowest mass flow rate is favorable during the charging process because it results in the smallest thermocline thickness for both temperature differences.

Moreover, Figure 2 (a) and (b) reflects that increasing the inlet temperature reduces the thermocline thickness at the two lowest mass flow rate of 2600 kg/h and 3000 kg/h, while at the highest mass flow of 3900 kg/h the thermocline thickness increases with the inlet temperature.

This suggest that for the latent-sensible heat TES configuration, a low charge rate and relatively low inlet temperature (but higher than the melting point of the PCM) is recommended. Similar findings was indicated by Bédécarrats et al. [18] for a TES filled with encapsulated PCM.
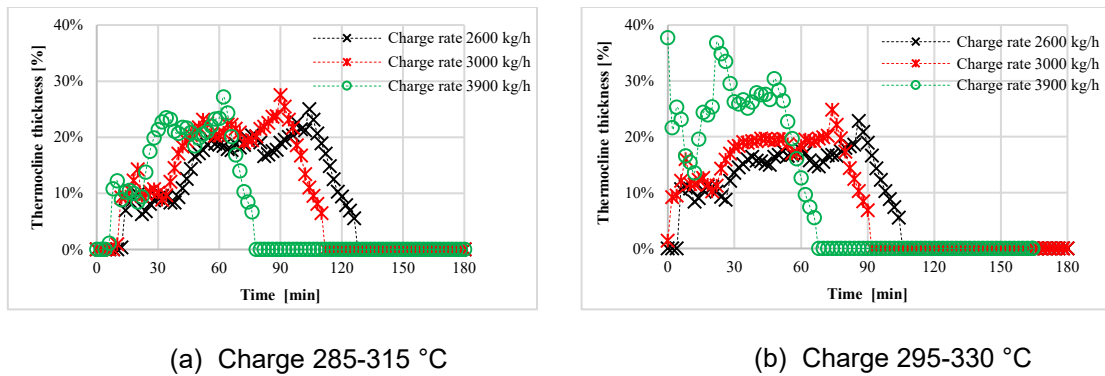

(a) Charge 285-315 °C   (b) Charge 295-330 °C

Figure 2. Thermocline thickness during charge.

During the discharge, Figure 3 evaluates the thermocline thickness at three discharge HTF mass flow rates 1600, 2000, and 3000kg/h with two temperature differences (a) 315 - 220°C and (b) 330 - 225°C. Similar to the charge, during the discharge process the thermocline thickness reduces with the increase in the discharge rate. However, comparing Figure 3 (a) and (b) suggests that the thermocline thickness has a similar behavior when the inlet temperature difference increases.
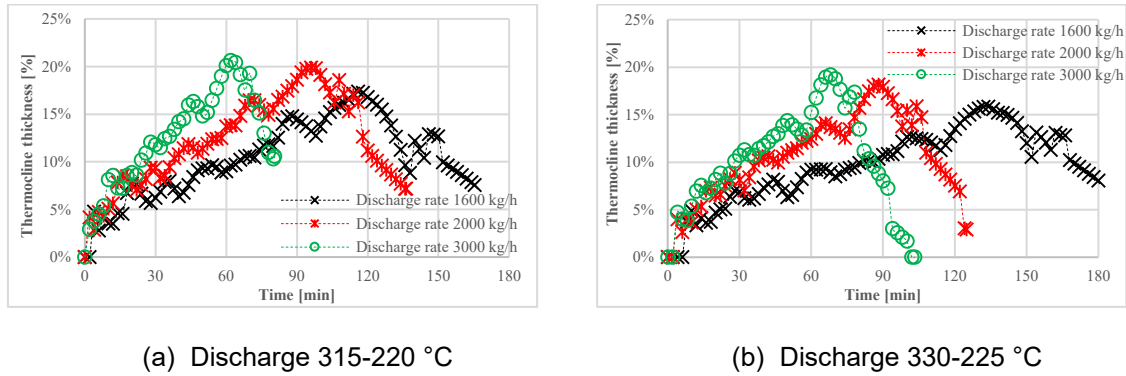

(a) Discharge 315-220 °C   (b) Discharge 330-225 °C

Figure 3. Thermocline thickness during discharge.

The comparison of Figure 2 and Figure 3 shows that the thermocline thickness is smaller during discharge process than charge process. This could be attributed to the PCM phase-change influence, as illustrated in Figure 4.

(1)   The thermocline starts to form and moves up with the HTF direction.
(2)   The thermocline expands, and the hot thermal front moves faster than the cold thermal front [2].
(3)   The hot thermal front reaches the PCM layer at the tank top, where the PCM stops it from moving up due to the phase-change.
(4)   The hot thermal front remains still, or progresses slowly due to the phase-change, while the cold thermal front moves up quickly to the PCM zone, and thus, the thickness is reduced.
(5)   The phase change is finished, so both the hot and cold thermal front move up further until the end of the process.
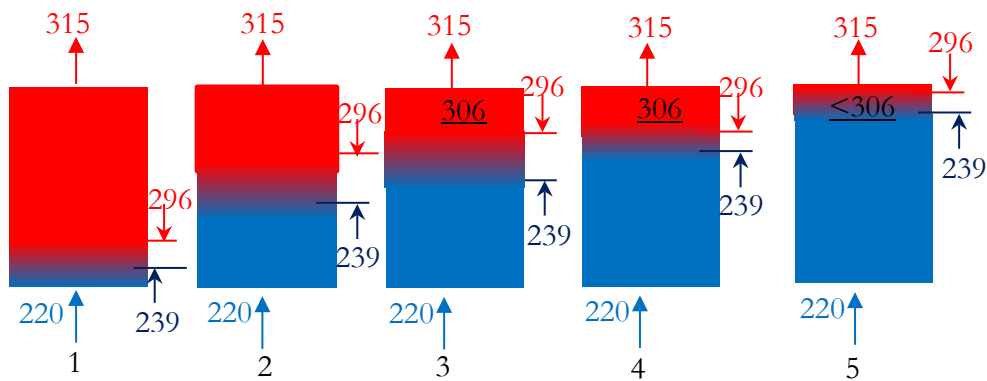

Figure 4. Depiction of thermocline thickness development during discharge.

4.2 Charge efficiency

Figure 5 plots the charge efficiency against time for the two evaluated temperature differences (a) 285 – 315 °C and (b) 295 -330°C. The figure illustrates that the charge efficiency does not exhibit significant changes in response to the rate change nor the temperature difference.
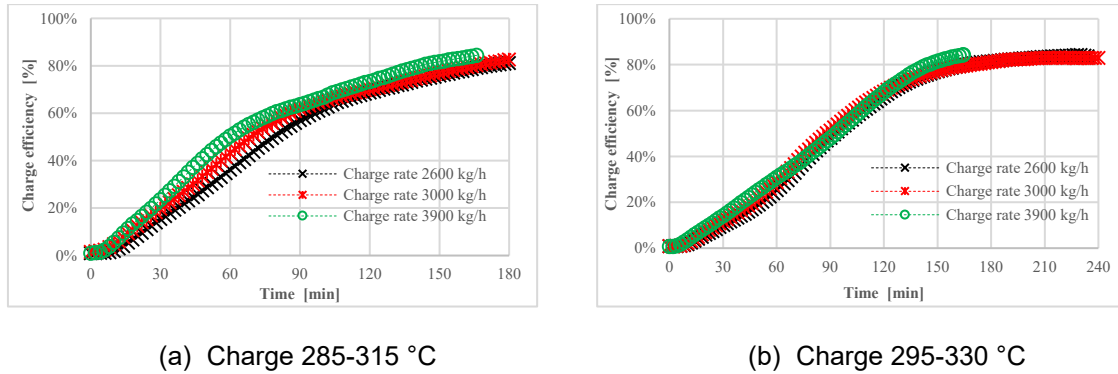

(a) Charge 285-315 °C   (b) Charge 295-330 °C

Figure 5. Charge efficiency.

4.3 Discharge efficiency

Figure 6 compares the efficiency during discharge with the three tested HTF mass flow rates 1600, 2000, and 3000kg/h at two temperature differences (a) 315 - 220°C and (b) 330 - 225°C. The figure indicates that the maximum discharge efficiency could be obtained at about the discharge rate of 2000 kg/h. This suggest that an optimal mass flow rate could be achieved for operating the TES unit. A similar finding was found by Hoffmann et al. [19].

Increasing the maximum operating temperature during discharge does not influence the order of magnitude of the discharge efficiency.
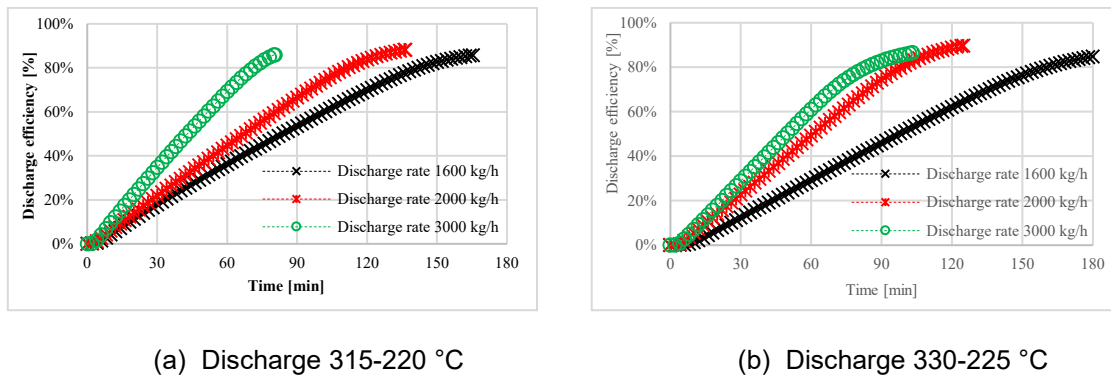

(a) Discharge 315-220 °C   (b) Discharge 330-225 °C

Figure 6. Discharge efficiency.

5. Conclusions

This work provides an experimental evaluation of the performance of a thermocline TES combining a 5.5% of $NaNO_3$ as PCM, to an alumina spheres. It is found that low mass flow rates are favorable during the charging and discharging because they result in reducing the thermocline thickness. Moreover, thermocline thickness during discharge is smaller than during charge, which suggests that the solidification of the PCM helped in reducing the thermocline thickness during discharge. While the efficiency of charging process does not show a signifi-

cant influence of the tested operating temperature nor the charge rates, the discharge efficiency improves with low discharge rates. Furthermore, the operating temperature has no significant influence on the discharge efficiency in the tested ranges.

Data availability statement

Not applicable.

Underlying and related material.

Not applicable.

Author contributions

Conceptualization by G. FLAMANT and J-J. BÉZIAN. Data curation by M. A. KEILANY. Formal analysis M. A. KEILANY, G. FLAMANT, M. MILHÉ, Q. FALCOZ, and J-J. BÉZIAN. Funding acquisition G. FLAMANT and J-J. BÉZIAN. Investigation M. A. KEILANY. Methodology M. A. KEILANY, G. FLAMANT, M. MILHÉ, Q. FALCOZ, and J-J. BÉZIAN. Project administration G. FLAMANT, J-J. BÉZIAN. Resources M. A. KEILANY and Q. FALCOZ. Software M.A. KEILANY and M. MILHÉ. Supervision M. MILHÉ, Q. FALCOZ. Validation M. A. KEILANY, G. FLAMANT, M. MILHÉ, Q. FALCOZ, and J-J. BÉZIAN. Visualization M. A. KEILANY. Writing - original draft M. A. KEILANY. Writing - review & editing M. A. KEILANY, G. FLAMANT, M. MILHÉ, Q. FALCOZ.

Competing interests

The authors declare no competing interests.

Funding

Acknowledgement

References

1. N. B. Desai, M. E. Mondejar, and F. Haglind, "Techno-economic analysis of two-tank and packed-bed rock thermal energy storages for foil-based concentrating solar collector driven cogeneration plants," Renew. Energy, vol. 186, pp. 814–830, 2022.
2. M. A. Keilany, M. Milhé, J. Bézian, Q. Falcoz, and G. Flamant, "Experimental evaluation of vitrified waste as solid fillers used in thermocline thermal energy storage with parametric analysis," J. Energy Storage, vol. 29, no. February, p. 101285, 2020.
3. N. Ahmed, K. E. Elfeky, L. Lu, and Q. W. Wang, "Thermal and economic evaluation of thermocline combined sensible-latent heat thermal energy storage system for

medium temperature applications," Energy Convers. Manag., vol. 189, no. March, pp. 14–23, 2019.

4. A. B. Hernández, I. Ortega-fernández, I. Uriz, A. Ortuondo, I. Loroño, and J. Rodriguez-aseguinolaza, "Parametric Analysis and Optimization of a Combined Latent-Sensible Packed Bed," SolarPaces Conf., 2017.

5. G. Zanganeh, M. Commerford, A. Haselbacher, A. Pedretti, and A. Steinfeld, "Stabilization of the outflow temperature of a packed-bed thermal energy storage by combining rocks with phase change materials," Appl. Therm. Eng., vol. 70, no. 1, pp. 316–320, 2014.

6. G. Zanganeh, R. Khanna, C. Walser, A. Pedretti, A. Haselbacher, and A. Steinfeld, "Experimental and numerical investigation of combined sensible-latent heat for thermal energy storage at 575 Deg C and above," Sol. Energy, vol. 114, pp. 77–90, 2015.

7. M. A. Keilany, S. Vannerem, M. Milh, Q. Falcoz, and G. Flamant, "Experimental and numerical study of combining encapsulated phase change material to sensible heat storage material in one-tank pilot scale thermal energy storage," vol. 51, no. November 2021, 2022.

8. S. A. Mohamed et al., "A review on current status and challenges of inorganic phase change materials for thermal energy storage systems," Renew. Sustain. Energy Rev., vol. 70, no. December 2016, pp. 1072–1089, 2017.

9. S. Pincemin, R. Olives, X. Py, and M. Christ, "Highly conductive composites made of phase change materials and graphite for thermal storage," Sol. Energy Mater. Sol. Cells, vol. 92, no. 6, pp. 603–613, 2008.

10. E. Rojas, R. Bayón, and E. Zarza, "Liquid Crystals: A Different Approach for Storing Latent Energy in a DSG Plant," Energy Procedia, vol. 69, pp. 1014–1022, 2015.

11. S. Kuravi, J. Trahan, D. Y. Goswami, M. M. Rahman, and E. K. Stefanakos, "Thermal energy storage technologies and systems for concentrating solar power plants," Prog. Energy Combust. Sci., vol. 39, no. 4, pp. 285–319, 2013.

12. S. H. Goods and R. W. Bradshaw, "Corrosion of Stainless Steels and Carbon Steel by Molten Mixtures of Commercial Nitrate Salts," ASM Int., vol. 13, no. February, pp. 78–87, 2003.

13. M. MUNRO, "Evaluated Material Properties for a Sintered alpha-Alumina," J. Am. Ceram. Soc., vol. 80, no. 8, pp. 1919–1928, 2005.

14. R. Anderson, S. Shiri, H. Bindra, and J. F. Morris, "Experimental results and modeling of energy storage and recovery in a packed bed of alumina particles," Appl. Energy, vol. 119, pp. 521–529, 2014.

15. S. Bellan et al., "Numerical analysis of charging and discharging performance of a thermal energy storage system with encapsulated phase change material," Appl. Therm. Eng., vol. 71, no. 1, pp. 481–500, 2014.

16. T. Fasquelle, Q. Falcoz, P. Neveu, and J. F. Hoffmann, "A temperature threshold evaluation for thermocline energy storage in concentrated solar power plants," Appl. Energy, vol. 212, no. January, pp. 1153–1164, 2018.

17. A. M. Bonanos and E. V. Votyakov, "Sensitivity analysis for thermocline thermal storage tank design," Renew. Energy, vol. 99, pp. 764–771, 2016.

18. J. P. Bédécarrats, J. Castaing-Lasvignottes, F. Strub, and J. P. Dumas, "Study of a phase change energy storage using spherical capsules. Part I: Experimental results," Energy Convers. Manag., vol. 50, no. 10, pp. 2527–2536, 2009.

19. J.-F. Hoffmann, T. Fasquelle, V. Goetz, and X. Py, "Experimental and numerical investigation of a thermocline thermal energy storage tank," Appl. Therm. Eng., vol. 114, pp. 896–904, 2017.